Evaporation-Induced Self-Assembly of Mesoscopically Ordered Organic/Organosilica Nanocomposite Thin Films with Photoluminescent Properties and Improved Hardness

Md. A. Wahab, Sundarraj Sudhakar,† Elaine Yeo, and Alan Sellinger*

*Institute of Materials Research and Engineering (IMRE) and the Agency for Science, Technology and Research (A*STAR), 3 Research Link, Singapore 117602, Republic of Singapore*

Received September 26, 2007. Revised Manuscript Received November 30, 2007

We report the use of evaporation-induced self-assembly (EISA) to organize and chemically bind a functionalized organic material, *N*,*N*′-bis(4-*tert*-butylphenyl)-*N*,*N*′-bis(4-((*E*)-2-(triethoxysilyl)vinyl)phenyl)biphenyl-4,4′-diamine (**3**), into the ordered nanochannels within an organosilica matrix based on 1,2-bis(triethoxysilyl)ethane (BTSE). Characterization techniques such as X-ray diffraction (XRD), transmission electron microscopy (TEM), thermogravimetric analysis (TGA), and nitrogen absorption/desorption (BET) were used to show that the EISA derived thin films and powders are highly ordered with compound **3** occupying and chemically bound within the nanochannels. Furthermore, photoluminescent spectroscopy (PL) and nanoindentation show these materials have unique PL properties with hardness values twice of their nonordered counterparts.

1. Introduction

Evaporation-induced self-assembly (EISA) has emerged as a technique to efficiently prepare nanostructured thin films with properties well suited for a variety of applications.[1–7] For example, functionalization of the nanochannels in mesoporous silica films with specific organic groups has recently received interest for shape and size selective surface catalysis,[8–10] membranes,[11–13] hard coatings,[4] optical hosts,[4] microfluidics,[13] low dielectric thin films,[7,14,15] sensing of biological and chemical analytes,[16,17] fundamental studies involving confined surface chemical and biochemical reactions,[1–3,18] and others toward the design of functional mesostructured materials.[1–3,19–25] A great deal of work has been reported on powder-based functionalized mesoporous solids having the active group attached to the pore surface or embedded in the pore walls.[27–35] Relatively much less activity on functionalized mesoporous thin films has been reported which presents a great opportunity in many ad-

* Corresponding author: e-mail alan-sellinger@imre.a-star.edu.sg, Tel 65 6874 4153, Fax 65 6872 7528.

† Present address: BASF South East Asia Pte Ltd, Competence Center for Nanostructured Surfaces, No. 61, Science Park Road, # 03-01 The Galen, Singapore Science Park III, Singapore 117525.

(1) Kapoor, M. P.; Inagaki, S. *Bull. Chem. Soc. Jpn.* **2006**, *79*, 1463.
(2) Grosso, D.; Cagnol, F.; Soler-Ilia, G. J. A. A.; Crepaldi, E. L.; Amenitsch, H.; Brunet, A. B.; Bourgeos, A.; Sanchez, C. *Adv. Funct. Mater.* **2004**, *14*, 309.
(3) Soler-Ilia, G. J. A. A.; Sanchez, C.; Lebeau, B.; Patarin, J. *Chem. Rev.* **2002**, *102*, 4093.
(4) Sellinger, A.; Weiss, P. M.; Nguyen, A.; Lu, Y.; Assink, R. A.; Gong, W.; Brinker, C. J. *Nature (London)* **1998**, *394*, 256.
(5) Lu, Y.; Yang, A.; Sellinger, A.; Lu, M.; Huang, J.; Fan, H.; Haddad, R.; Lopez, G.; Burns, A. R.; Sasaki, D. Y.; Shelnutt, J.; Brinker, C. J. *Nature (London)* **2001**, *410*, 913.
(6) Brinker, C. J.; Lu, Y.; Sellinger, A.; Fan, H. *Adv. Mater.* **1999**, *11*, 579.
(7) Lu, Y.; Fan, H.; Doke, N.; Loy, D. A.; Assink, R. A.; LaVan, D. A.; Brinker, C. J. *J. Am. Chem. Soc.* **2000**, *122*, 5258.
(8) Sharma, K. K.; Asefa, T. *Angew. Chem., Int. Ed.* **2007**, *46*, 2879.
(9) Nakajima, K.; Tomita, I.; Hara, M.; Hayashi, S.; Doem, K.; Kondu, J. N. *Adv. Mater.* **2005**, *17*, 1839.
(10) Xing, R.; Lie, N.; Liu, Y.; Wu, H.; Liang, Y.; Chen, L.; He, M. *Adv. Funct. Mater.* **2007**, *17*, 2455.
(11) Athens, G. L.; Eli, Y. E.; Chmelka, B. F. *Adv. Mater.* **2007**, *19*, 2580.
(12) Yilma, S.; Liu, N.; Samoylov, A.; Lo, T.; Brinker, C. J.; Vodyanoy, V. *Biosen. Bioelectron.* **2007**, *22*, 1605.
(13) Liu, N.; Dunphy, D. R.; Atanassov, P.; Bunge, S.; Chen, Z.; Lopez, G. P.; Boyle, T. J.; Brinker, C. J. *Nano Lett.* **2004**, *4*, 551.
(14) Dag, O.; Ishii, C. Y.; Asefa, T.; McLachlan, M. J.; Grondey, H.; Coombs, N.; Ozin, G. A. *Adv. Funct. Mater* **2001**, *11*, 213.
(15) Hatton, B. D.; Landskron, K.; Whitnall, W.; Perovic, D. D.; Ozin, G. A. *Adv. Funct. Mater.* **2005**, *15*, 823.
(16) Patel, A. C.; Yuan, J. M.; Wei, Y. *Nano Lett.* **2006**, *6*, 1042.
(17) Nazeeruddin, M. K.; Censo, D.; Baker, R. H.; Gratzel, M. *Adv. Funct. Mater.* **2006**, *16*, 189.
(18) Angelome, P. C.; Soller-Ilia, G. J. A. A. *Chem. Mater.* **2005**, *17*, 322.
(19) Wahab, M. A.; Sellinger, A. *Chem. Lett.* **2006**, *11*, 1240.
(20) Ogawa, M. *J. Am. Chem. Soc.* **1994**, *116*, 7941.
(21) Minoofar, P. N.; Hernandez, R.; Chia, S.; Dunn, B.; Zink, J. I. *J. Am. Chem. Soc.* **2001**, *123*, 1248.
(22) Minoofar, P. N.; Hernandez, R.; Chia, S.; Dunn, B.; Zink, J. I.; Franville, A. C. *J. Am. Chem. Soc.* **2004**, *124*, 14388.
(23) Aida, T.; Tajima, K. *Angew. Chem., Int. Ed.* **2001**, *40*, 3803.
(24) Yang, P.; Wirnsberger, G.; Huang, H. C.; Cordero, S. R.; McGehee, M. D.; Scott, B.; Deng, T.; Whitesides, G. M.; Chmelka, B. F.; Buratto, S. K.; Stucky, G. D. *Science* **2000**, *287*, 465.
(25) Miyata, H.; Suzuki, T.; Fukuoka, A.; Sawada, T.; Watanabe, M.; Noma, T.; Takada, K.; Mukaide, T.; Kuroda, K. *Nat. Mater.* **2004**, *651*, 651.
(26) Zulkalova, M.; Zukul, A.; Kavan, L.; Nazeeruddin, M. K.; Liska, P.; Gratzel, M. *Nano Lett.* **2005**, *5*, 1789.
(27) Lim, M. H.; Stein, A. *Chem. Mater.* **1999**, *11*, 3285.
(28) Burkett, S. L.; Sims, S. D.; Mann, S. *Chem. Commun.* **1996**, 1367.
(29) Yang, Q.; Kapoor, K. P.; Inagaki, S. *J. Am. Chem. Soc.* **2002**, *124*, 9694.
(30) Markowitz, M. A.; Klaehn, J.; Hendel, R. A.; Qadriq, S. B.; Golledge, S. L.; Castner, D. G.; Gaber, B. P. *J. Phys. Chem B* **2000**, *651*, 10820.
(31) Huh, S.; Wiench, J. W.; Yoo, J. C.; Pruski, M.; Lin, V. Y. S. *Chem. Mater.* **2003**, *15*, 4247.
(32) Raynhardt, J. K. P.; Yang, Y.; Sayari, A.; Alper, H. *Chem. Mater.* **2004**, *16*, 4095.
(33) Wahab, M. A.; Imai, I.; Kawakami, Y.; Ha, C. S. *Chem. Mater.* **2005**, *17*, 2165.
(34) Wahab, M. A.; Ha, C. S. *J. Mater. Chem.* **2005**, *15*, 508.
(35) Jin, X.; Hu, Q.; Hampsey, J. E.; Qiu, X.; Gao, L.; He, J.; Lu, Y. *Chem. Mater.* **2006**, *18*, 2265.

10.1021/cm702753b CCC: $40.75
Published on Web 01/23/2008

Scheme 1. Synthetic Preparation of Photoluminescent/Charge Transport Molecule *N*,*N*′-Bis(4-*tert*-butylphenyl)-*N*,*N*′-bis(4-((*E*)-2-(triethoxysilyl)vinyl)phenyl)biphenyl-4,4′-diamine) (3)[a]

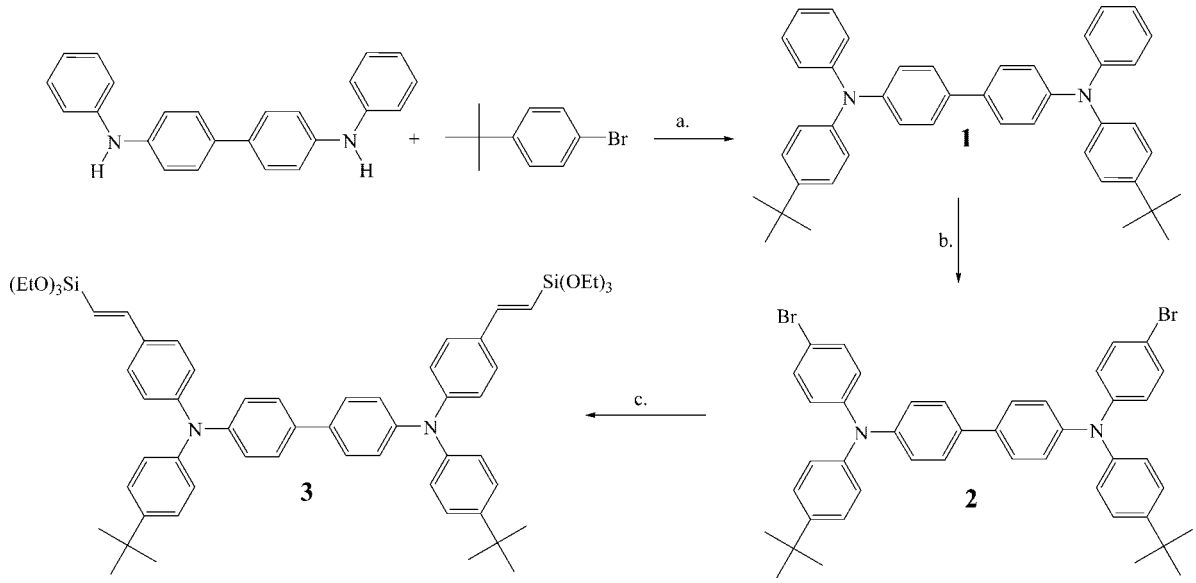

[a] a: Pd[P(tBu)$_3$]$_2$, NaOtBu, toluene, 80°C, 8 h, >80% yield; b: *N*-bromosuccinimide, DMF, 8 h, 98% yield; c: Pd[P(tBu)$_3$]$_2$, NCH$_3$Cy$_2$, vinyltriethoxysilane, toluene, 80°C, 8 h, 94% yield.

vanced applications such as solar cells, coatings, and sensors to name a few.[4,12,18,26]

In this article, we report an approach that combines periodic mesoporous organosilica (PMO)[36–39] and EISA to fabricate photoluminescent (PL) and charge transport (CT) functionalized nanocomposite thin films in situ wherein the PL/CT material is confined and chemically bonded inside the nanochannels. Furthermore, we show that the hardness of resultant ordered films is 5 times greater than that of the organosilica matrix alone and 2 times greater than their nonordered counterparts. Our strategy is to use 1,2-bis(triethoxysilyl)ethane (BTSE) as the organosilica matrix, and a reactive hydrophobic PL/CT material that could be positioned into the hydrophobic portion of the micelle during the EISA process and subsequently chemically bonded to the inner nanochannel pore wall surface. We chose BTSE over tetraethyl orthosilicate (TEOS) as it more consistently forms defect-free thin films under the conditions used in this study. The nanocomposite materials are then washed with hot ethanol and THF to remove the surfactants and residual unbound PL/CT materials, leaving behind the active PL/CT material confined within the nanochannels of the organosilica matrix. The EISA method to in situ fill the nanochannels in this type of material is advantageous in that all pores from substrate to air interface can be filled. In other approaches such as solution or melt infiltration, the complete filling of the total pore network is difficult and requires more steps. Furthermore, using an infiltration method with sol–gel

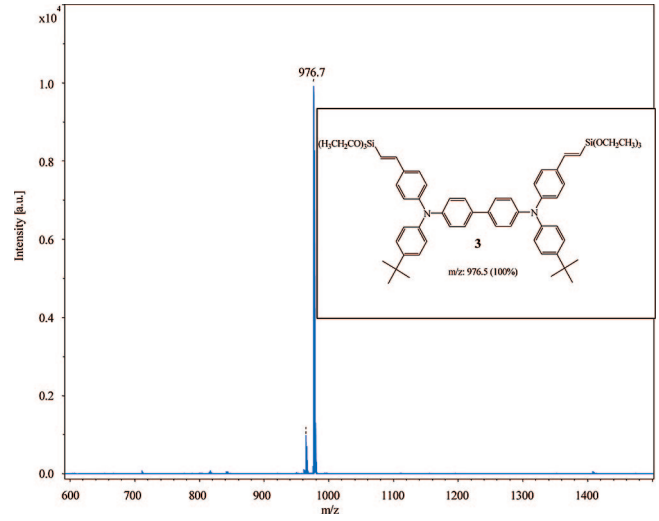

Figure 1. MALDI-TOF spectrum of compound **3**.

functionalized materials may result in reactions occurring at the pore entrance, thus blocking further material from entering the channels.

It is anticipated that the emission and charge transport properties of the active organic material could be greatly affected by their confinement within the nanochannels which may be well suited for organic electronic applications such as light-emitting diodes, solar cells, and thin film transistors.[26] For example, the confinement of compound **3** or similarly functionalized analogues within a lamellar sheet or 1-D hexagonal channel on the order of 2–3 nm could provide a nontortuous path for charges to move, thus the possibility for higher charge mobility thin films versus their bulk counterparts. Additionally, isolation in the nanochannels would prevent the aggregation and/or $\pi-\pi$ stacking of molecules, often responsible for charge trapping and broadening of luminescence due to eximer formation.

(36) Inagaki, S.; Guan, S.; Fukushima, Y.; Ohsuna, T.; Terasaki, O. *J. Am. Chem. Soc.* **1999**, *121*, 9611.
(37) Melde, B. J.; Holland, B. T.; Blanford, C. F.; Stein, A. *Chem. Mater.* **1999**, *11*, 3302.
(38) Asefa, T.; MacLachlan, M. J.; Coombs, N.; Ozin, G. A. *Nature (London)* **1999**, *402*, 867.
(39) Yoshina-Ishii, C.; Asefa, T.; Coombs, N.; MacLachlan, M. J.; Ozin, G. A. *Chem. Commun.* **1999**, 2539.

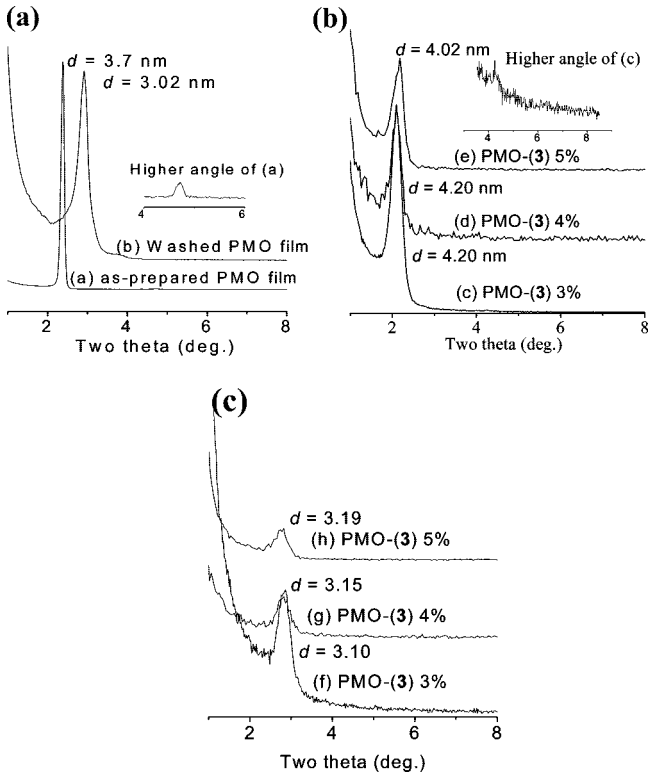

Figure 2. High-resolution X-ray diffraction patterns of (a) as-prepared and ethanol-washed PMO films, (b) PMO-(**3**) films, and (c) ethanol-washed PMO-(**3**) films. In (b) and (c) the number at the end (3, 4, 5) refers to wt % of **3** in the initial solutions.

Table 1. Nitrogen Sorption Properties of Pure and Functionalized PMO Materials Derived from the EISA Process

sample	BET[a] (m^2/g)	PV[b] (cm^3/g)	PSD[c] (nm)
as-prepared PMO	25	0	N/A[d]
washed PMO	1074	0.80	2.5
calcined PMO	1037	0.72	2.6
PMO-(**3**) (3%)	690	0.52	2.0
PMO-(**3**) (4%)	648	0.40	1.5
PMO-(**3**) (5%)	356	0.19	1.5

[a] BET surface areas; surface area and total pore volume reduction for functionalized PMOs with respect to washed PMO. [b] Total pore volume. [c] BJH pore size. [d] Not applicable.

Lastly, as the nanochannels are filled within the ordered thin film, any defect initiated from either interface would quickly be deflected and interrupt further propagation to result in potentially harder films over their nonordered counterparts. Such properties would have applications for abrasion-resistant coatings and packaging to minimize moisture and oxygen permeation.

2. Experimental Section

Materials and Methods. 1,2-Bis(triethoxysilyl)ethane (BTSE) and cetyltrimethylammonium bromide (CTAB) were purchased from Aldrich and used as received. All materials used for the synthesis of **3** were commercial products (Aldrich, Fluka, TCI, Strem, Acros, Avocado) and were used as received. All chemical synthetic reactions were carried out using Schlenk techniques in an argon atmosphere with anhydrous solvents.

Preparation of Periodic Mesoporous Organosilica Precursor Sols, Thin Films, and Powders. BTSE, EtOH, water, and HCl (as 0.07 M HCl) in the following molar ratios (1.00:6.37:2.12:8.63 $\times$ 10^{-5}) were refluxed at 60 °C for 90 min to form the precursor stock solution that was used in all subsequent steps. The precursor solution was further diluted with tetrahydrofuran (THF), 0.07 M HCl, and water. CTAB was added to the dilute solutions to prepare 3 wt % concentrations. Compound **3** (Scheme 1) was added to prepare 3, 4, and 5 wt % solutions. Final molar ratios of a 5 wt % of **3** were as follows: BTSE:EtOH:H_2O:HCl:THF:CTAB:**3** (1.00:6.38:9.08:6.63 $\times$ 10^{-3}:22.4:0.22:0.14).

Thin films were prepared by spin-coating the solutions onto precleaned glass substrates. Powders were prepared by pouring the solutions into Petri dishes (10 cm diameter) followed by evaporation of the volatile components. All solutions were filtered through 0.45 μm PTFE syringe filters and spin-coated onto cleaned glass substrates at 1500 rpm. Prior to thin film deposition, the glass substrates were cut into 2.5 cm^2 pieces, submerged in 1 M H_2SO_4, and ultrasonicated for 1 h. The substrates were next ultrasonicated for 30 min each in deionized water, acetone, and isopropyl alcohol. The deposited thin films and powders were heat-treated at 80 °C for 12–14 h followed by washing with ethanol for 10 min (thin films), 18 h using ethanol in a Sohxlet extractor (powders) to remove CTAB, and 6 h stirring in THF to remove any unreacted **3**. Samples were then heat treated at 80 °C for 2 h prior to characterization. Calcination was performed by heating pure PMO samples in air from room temperature to 425 °C at a rate of 1 °C/min and holding at 425 °C for 4 h.

Synthesis of Luminescent Sol–Gel Precursor Synthesis. *N,N′-Bis(4-tert-butylphenyl)-N,N′-bis(phenyl)biphenyl-4,4′-diamine (**1**).* A flame-dried flask was charged with NaOtBu (5.8 g, 60 mmol) and dried at 110 °C under vacuum for 1 h. After cooling to room temperature, 4,4′-dibromobiphenyl (3.12 g, 10 mmol), aniline (1.83 mL, 20 mmol), and $Pd[P(tBu)_3]_2$ (25.5 mg, 5 $\times$ 10^{-2} mmol) were added followed by 40 mL of toluene. The reaction mixture was purged using argon for a few minutes and then heated to 70 °C under an argon atmosphere until all the amine was consumed as monitored by thin layer chromatography (TLC). The reaction mixture was then cooled to room temperature followed by the addition of 4-bromo-*tert*-butylbenzene (3.47 mL, 20 mmol), $PdP(tBu)_3]_2$ (25 mg, 5 $\times$ 10^{-2} mmol), and additional toluene (20 mL). The reaction mixture was stirred at 90 °C for 15 h, cooled to room temperature, and extracted with water. The organic layer was dried with $MgSO_4$ and concentrated to obtain an oily residue which was precipitated in methanol to obtain a gray solid that was filtered and dried. The product obtained was used in the next step without any further purification. Yield >80%.

*N,N′-Bis(4-tert-butylphenyl)-N,N′-bis(4-bromophenyl)biphenyl-4,4′-diamine (**2**).* To a solution of **1** (4.9 g, 8.33 mmol) in 300 mL of DMF was added dropwise at room temperature a solution of *N*-bromosuccinimide (NBS) (2.97 g, 16.7 mmol) in 100 mL of DMF. The reaction mixture was stirred at room temperature overnight. The reaction mixture was precipitated by pouring into acidified water, filtered, washed thoroughly with water, and dried. Yield 98%. The product obtained was shown to be quite pure from MALDI-TOF and used in the next step without any further purification.

*N,N′-Bis(4-tert-butylphenyl)-N,N′-bis(4-((E)-2-(triethoxysilyl)vinyl)phenyl)biphenyl-4,4′-diamine (**3**).* To a flame-dried flask was added **2** (1.9 g, 2.5 mmol), $Pd[P(tBu)_3]_2$ (25.5 mg, 5 $\times$ 10^{-2} mmol), and 10 mL of dioxane. To this solution were added vinyltriethoxysilane (1.3 mL, 6.25 mmol) and an argon degassed solution of dicyclohexylmethylamine (1.35 mL, 6.25 mmol). The reaction mixture was stirred at 80 °C overnight and then cooled and filtered to remove the amine hydrochloride salt. Dioxane was removed on a rotary evaporator to afford the crude product which was redissolved in ethyl acetate and extracted with cold 5% HCl three times and then with a saturated NaCl solution. The organic layer

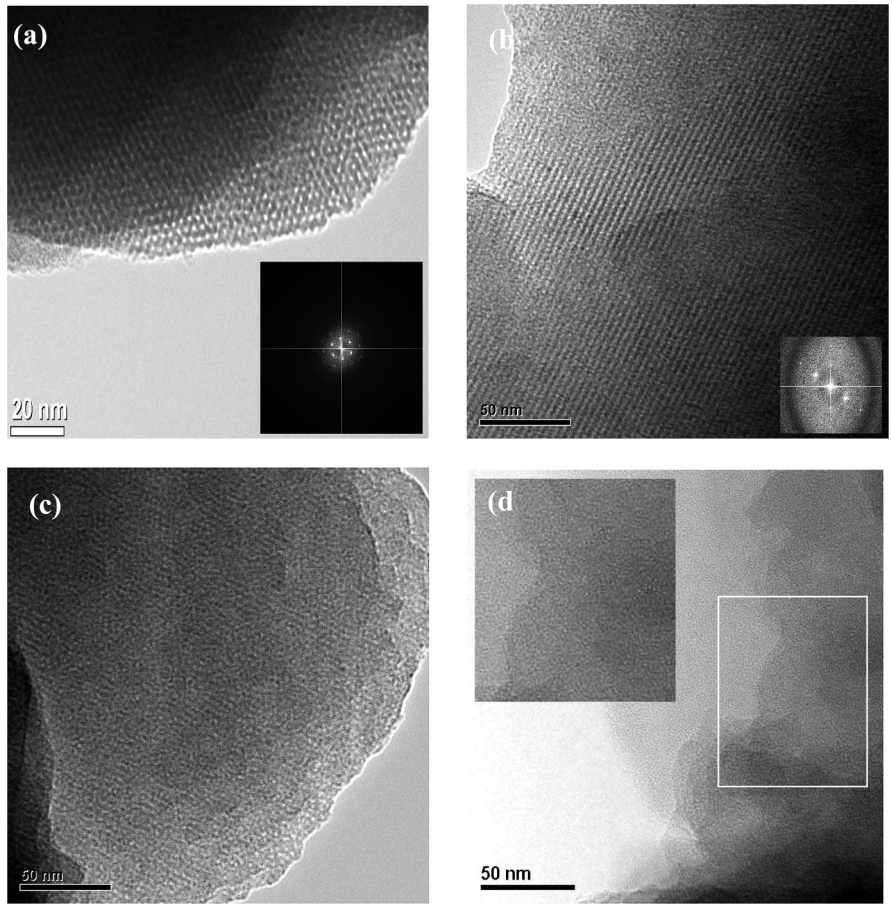

Figure 3. HR-TEM images of ethanol-extracted (a) pores of pure PMO with pores, (b) pure PMO with ordered pore channels, (c) PMO-(**3**) (4%), and (d) PMO-(**3**) (5%). The inset (a, b) is a representative electron diffraction pattern of PMO.

was then dried over anhydrous $MgSO_4$, filtered, concentrated, and precipitated in methanol to provide a bright yellow solid. Yield 2.3 g, 94%. ^{1}H NMR (CD_2Cl_2): δ = 1.26 (t, 18H, J = 7.0 Hz), 1.34 (s, 18H), 3.87 (q, 12 H, J = 7.0 Hz), 6.03 (d, 2H, J = 19.2 Hz), 7.05 (d, 4H, J = 8.8 Hz), 7.08 (d, 4H, J = 8.4 Hz), 7.14 (d, 4H, J = 8.4 Hz), 7.15 (d, 2H, J = 19.2 Hz), 7.34 (d, 4H, J = 8.4 Hz), 7.38 (d, 4H, J = 8.8 Hz), 7.50 (d, 4H, J = 8.8 Hz). ^{13}C NMR (CD_2Cl_2): δ = 18.43, 31.52, 58.83, 115.90, 122.98, 124.76, 125.19, 126.66, 127.63, 127.97, 132.04, 135.40, 144.90, 146.96, 147.28, 148.58, 148.86. MS (MALDI TOF): *m*/*z* 976.7 (100%), calcd for $C_{60}H_{76}N_2O_6Si_2$: 976.5 (100%).

Characterization Techniques. Solution ^{1}H and ^{13}C NMR were performed on a Bruker DPX 400 MHz spectrometer with chemical shifts referenced to CD_2Cl_2. Solid-state NMR spectra were recorded on the same NMR instrument equipped with solid-state probe using the following experimental conditions: ^{13}C CP/MAS NMR, 6 μs prescan delay time, 2000 μs contact pulse, 5 kHz MAS rate, and 2000 scans; ^{29}Si CP/MAS NMR, 30.0 μs delay time, 1200 μs contact pulse, 5 kHz MAS rate, and 2500 scans. MALDI-TOF mass spectra were obtained on a Bruker Autoflex TOF/TOF instrument using dithranol as the matrix. Ceramic yields and decomposition temperatures were determined by thermogravimetric analysis using a TA Instruments TGA Q500 in hi-res mode with a heating rate 10 °C min^{-1} from 50 to 950 °C.

All EISA-derived materials were characterized by high-resolution X-ray diffraction at low incidence angles in the X-ray demonstration and development (XDD) beamline at the Singapore Synchrotron Light Source (SSLS). A Huber four-circle system 90000-0216/0 diffractometer with high-precision 0.0001° step size for omega and 2θ circles was used. The distance from entrance slit to sample center was 688 mm, and that from sample center to detector was 680 mm. The storage ring, Helios 2, was running at 700 MeV and typically stored electron beam current of 300 mA. The X-ray beam was conditioned to select 8.048 keV photons by a Si(111) channel-cut monochromator (CCM) and blocked to be 1.00 mm high in the vertical direction and 3.50 mm wide in the horizontal direction by a collimating mirror and slit system. Such a setup yielded X-ray beams with about 0.01° in divergence at 8.048 keV. The detector slit was adjusted to be 1.00 mm high to ensure recording of all reflected photons. The typical counting time was 5 s for every step, and step size of 2θ varied from 0.01 to 0.02° for different samples to ensure that the diffraction peak was well recorded. Powder samples were analyzed using a small-angle Bruker D8 GADDS X-ray diffractometer. Sample surface areas and pore structures were determined by nitrogen sorption at 77 K using a Quantachrome BET surface area analyzer (model NOVA 1000) and applying the Brunauer–Emmett–Teller (BET) and Barret−Joyner−Halenda (BJH) methods. The pore-size distributions were evaluated from the desorption branch of the isotherm by use of the BJH method. All of the samples were dehydrated at 150 °C for 24 h prior to nitrogen adsorption experiments. TEM (Philips CM300 FEG TEM microscope; operated at 300 kV) images were obtained by dispersing sample particles using ultrasonication in methanol and then pouring the solution onto a holey carbon grid. Luminescent measurements were carried out using a Perkin-Elmer LS50B luminescence spectrometer . The PL exitation wavelength was selected from the UV_{max} absorption using a UV–vis photospectrometer (UV-3101PC). The nanoindentation tests were performed using MTS Nano XP with a Berkovich (three-side pyramid) indenter. A constant strain rate of 5% s^{-1} was applied during loading segment. A 60 s holding time was used after the indenter reached maximum depth. The same rate was applied for the unloading segment. The reported hardness

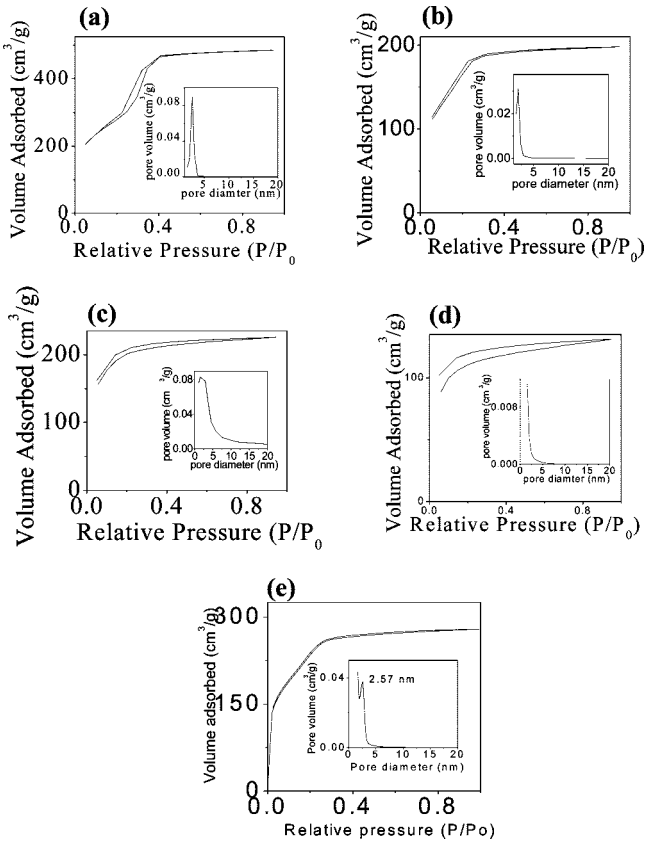

Figure 4. N_2 adsorption–desorption isotherms and pore size distribution (inset) of ethanol-washed (a) pure PMO, (b) PMO-(**3**) (3%), (c) PMO-(**3**) (4%), (d) PMO-(**3**) (5%), and (e) calcined pure PMO.

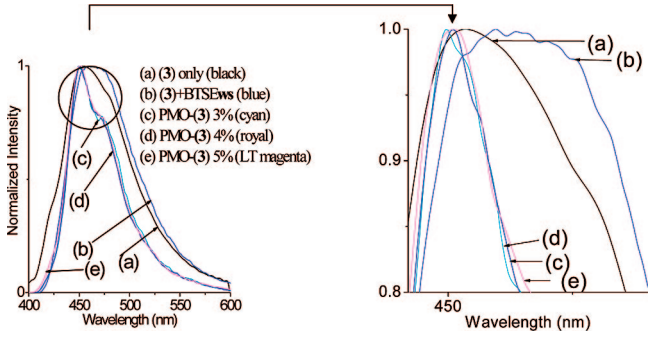

Figure 5. Photoluminescent spectra of pure PL/CT and PL/CT **3** functionalized PMO films on glass substrate: (a) as-prepared samples, (b) ethanol-washed samples, (c) PMO-(**3**) (3%), (d) PMO-(**3**) (4%), and (e) PMO-(**3**) (5%). In the figure, ws indicates "without surfactant".

values are averaged over a depth range from 20 to 75 nm where the total film thicknesses were 550–570 nm.

3. Results and Discussion

Scheme 1 shows the synthetic procedure for the new sol–gel reactive hydrophobic molecule with both PL and CT properties *N*,*N*′-bis(4-*tert*-butylphenyl)-*N*,*N*′-bis(4-((*E*)-2-(triethoxysilyl)vinyl)phenyl)biphenyl-4,4′-diamine (**3**). This procedure to attach triethoxysilane groups is very straightforward, introduces conjugation between Si and the aromatic portion, and tolerates many functional groups unlike traditional approaches that use organomagnesium or butyllithium chemistry.[40] Molecule **3** is hydrophobic in nature and not soluble in the traditional ethanol-based solvent systems used

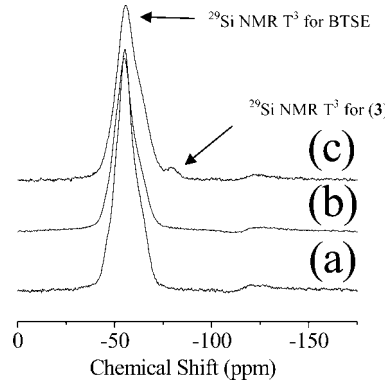

Figure 6. ^{29}Si CP MAS spectra (a) as-prepared PMO, (b) ethanol-washed pure PMO, and (c) ethanol-washed PMO-(**3**) (5%).

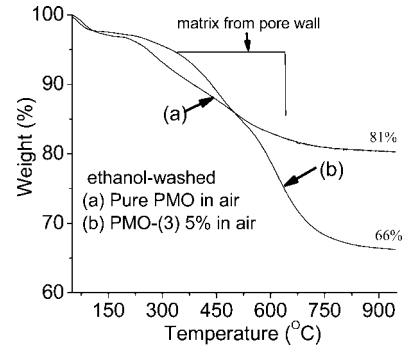

Figure 7. Thermal gravimetric analysis (TGA) in air of ethanol-washed pure PMO and PMO-(**3**) (5%).

Table 2. Hardness of Pure and Functionalized Periodic Mesoporous Organosilica Films

sample code	hardness (GPa)[a]
BTSE only	0.03
BTSE-(**3**) (3%) without CTAB	0.07
as-prepared PMO	0.03
washed PMO	0.05
as-prepared PMO-(**3**) (3%)	0.11
washed PMO-(**3**) (3%)	0.14

[a] Hardness values are the averaged values of at least five runs for each thin film.

for most EISA processes. As a result, we needed to reformulate our system to include THF in order to solubilize **3**. The six ethoxysilane groups on **3** are designed for eventual reaction with the hydroxylated nanopore wall surface. The aromatic amine structure is known for good hole transport properties in organic light-emitting diodes (OLEDs),[41] while the added conjugation from the vinylsilyl group provides red-shifted absorption (370 vs 352 nm) and PL (458 vs 408 nm) compared with molecules without extended conjugation. The MALDI-TOF spectrum of **3** confirms the molecular weight and is shown in Figure 1.

Initial sol–gel formulations that included ethanol only were not suitable as **3** was not soluble. Reformulation to replace 66% of the ethanol component with THF resulted in clear stable solutions that could be used for further processing of functionalized EISA-derived thin films and powders.

Figure 2 shows high-resolution XRD patterns of as-prepared and ethanol-washed PMO films. The as-prepared

(40) Shea, K. J.; Loy, D. A. *Chem. Mater.* **2001**, *13*, 3306.
(41) Hung, L. S.; Chen, C. H. *Mater. Sci. Eng. R* **2002**, *3*, 143.

PMO film without **3** in Figure 2a reveals a 2θ XRD peak at 2.38° and a second-order peak at 4.76°.[4,14,15] In the functionalized PMO films [PMO-(**3**)], the characteristic (100) peaks for mesophases are still observed, even after extensive solvent washing (ethanol and THF), and are consistent with CTAB functionalized mesoporous silica films.[20–23] The overall intensity of the (100) peak in the washed PMO-(**3**) is lower compared with washed PMO, suggesting some overall loss in ordering. This is not surprising considering the loadings and molecular size of **3** are likely to disrupt the ability for CTAB to form micelles and corresponding mesophases. In fact, a 12% loading of **3** into the formulation containing 3% CTAB resulted in a complete loss of the (100) reflection. As the loading of **3** increased from 0 to 5 wt %, the position of the main (100) reflection shifts to lower angles, corresponding to an increase in *d*-spacing from 3.70 to 4.20 nm and 3.03 to 3.15 nm for as-prepared and solvent-washed films, respectively. Such an increase in *d*-spacing likely results from the incorporation of **3** within the hydrophobic micellar cores of the liquid crystalline mesophases due to a "swelling effect".[21,22] The attenuation of the XRD peaks for functionalized films is due to the X-ray scattering contrast between the mesoporous organosilica walls and organic moieties that are inside the PMO nanochannels.[27–33] The anticipated contraction of *d*-spacing for solvent-washed samples is due to the removal of the surfactant and accompanying co-condensation of silanol (Si−OH) groups.[4] For comparison, powder (prepared from an EISA process) XRD diffraction patterns of ethanol and THF-washed powder samples were also carried out and show similar patterns to the thin films as shown in Table 1.

Transmission electron microscope (TEM) images obtained for ethanol-washed pure PMO and PMO-(**3**) are shown in Figure 3. The highly ordered periodic nanochannels in parts a and b of Figure 3 are in good agreement with the dimensions and pore sizes observed in XRD and BET data, respectively.[4,29] The obtained TEM image in Figure 3c for PMO-(**3**) further substantiates the incorporation of **3** into the PMOs and is consistent with XRD and BET data. Similar observations were made for other functionalized PMOs and mesoporous silicas.[27,28,33–35]

Nitrogen adsorption–desorption isotherms and pore size distribution analysis for ethanol- and THF-washed, pure, and functionalized PMOs [5 wt % **3**] were carried out and are shown in Figure 4. The washed and calcined PMO samples exhibited type IV isotherms with narrow and uniform pore size distributions and BET surface areas of 1074 and 1050 m^2/g, respectively. The obtained total pore volume by both processes were in the range 0.80−0.72 cm^3/g (see Table 1), indicating the efficiency of the ethanol and THF washing method.[15,27,29] The obtained shape of the isotherms for functionalized PMOs gradually changed from type IV to type I as the content of **3** increased, indicating that the pore sizes of all PMOs are changing with respect to loading.[30–35] As indicated in Table 1, surface areas, pore volumes, and pore sizes of PMOs gradually decreased as the amount of **3** was increased (3, 4, and 5 wt % in initial solutions), indicating that the pores are becoming filled.[27,32] This would not be the case if the PL material were simply integrated into the organosilica matrix. Furthermore, the additional washing with ethanol and THF did not change the surface area results, indicating that **3** is occupying the nanochannels and is chemically bound to the organosilica pore walls.

Thin films of various compositions were prepared and studied by PL emission spectroscopy, and the results are shown in Figure 5. For this study we prepared four sets of thin films: mesoporous PMO, pure **3**, amorphous organosilica + **3** (prepared without surfactant), and PMO-(**3**). As expected, the mesoporous PMO films without **3** showed no PL properties. Films from pure **3** showed a broad featureless PL spectrum with a maximum at 455 nm and full width at half-maximum of 77 nm. Films prepared from organosilica and **3** without surfactant (amorphous) show similar spectra as pure **3**. Thin films based on PMO-(**3**) show a 5 nm blue-shifted maximum PL of 450 nm with a significant shoulder at 475 nm. Additionally, these films have a much more narrow full width at half-maximum in the range of 53−56 nm. These results indicate that **3** in the PMOs are in a much different environment than the other nonordered films. We propose that this spectral difference is due to **3** being ordered and isolated within the nanochannels of PMOs.[21–23] This isolation would suppress the ability for **3** to form long-range aggregates that are often responsible for red-shifted and broad PL spectra.

The silicon atoms from **3** and BTSE are attached to differently hybridized carbon atoms. For example, the Si atom in **3** (−O3Si−*C*═C−) and BTSE (−O3Si−*C*−C−) are attached to sp^2 and sp^3 hybridized carbon atoms, respectively, and as a result should have different ^{29}Si chemical shifts. Experimentally, the solid-state ^{29}Si NMR spectra for the as-prepared and ethanol-washed PMO in Figure 6 show one large peak at –55 ppm with a shoulder around –65 ppm. These can be attributed to the T^2 and T^3 sites, respectively, for BTSE.[4,7,14,15] PMO-(**3**) reveals an additional peak at –79.5 ppm corresponding to the T^3 species. It is likely that the T^2species exists in the –68 to –70 ppm region but is overlapped with the main peak of BTSE.[14,15,27,29,31,33] The absence of Q^{3-4} silicon resonances between –90 and –120 ppm confirms that no cleavage of carbon−silicon bond [BTSE or **3**] has occurred during reaction.[14,15,31,35]

Thermogravimetric analyses (TGA) were carried out in air from 50 to 950 °C on solvent-extracted PMO and PMO-(**3**) and are shown in Figure 7. The TGA profiles show two weight loss steps: weight loss below 150 °C (≈2–3%) is due to the removal of physisorbed water which is common in these types of materials; weight loss between 200 and 950 °C can be assigned to the decomposition of loosely bound $Si-(OR)_{1-3}$ groups where R = H and/or CH_2CH_3 (200−350 °C) and then the organic matrix of both BTSE and **3** (350−950 °C).[32–35] The ceramic yields to SiO_2 for PMO and PMO-(**3**) are 81% and 66%, respectively. The PMO ceramic yield is quite close to theoretical values while the PMO-(**3**) value of 66% is slightly larger than expected. This is not surprising as during the EISA process it is likely that some **3** buried in the interior of the hydrophobic micelle is unable to reach and react with the silanol interface and is thus washed away during the hot ethanol Soxhlet extraction

process. In fact, the extraction solvent becomes slightly photoluminescent, indicating some **3** is being washed out.

In contrast to sol–gel derived disordered silica-based nanocomposite materials, very few examples on the mechanical properties of surfactant-mediated mesostructured silica materials have been reported.[4,7,15] In this regard, we have carried out nanoindentation experiments on various thin films deposited from spin-coating, and the results are shown in Table 2.[42] As the measurements were made over depth ranges from 20 to 75 nm, where the total film thicknesses were 550–570 nm, there should be no influence from the substrate. Here it is clearly observed that the washed ordered thin film nanocomposites PMO-(**3**) have the highest hardness values compared to all other films in this study. For example, the washed PMO-(**3**) films are 4.7 and 2.0 times harder than the nonordered BTSE and BTSE-**3** films, respectively. Furthermore, PMO-(**3**) is 2.8 times harder than the ordered PMO without **3**. This result provides more evidence that the pore channels are being occupied by **3**.

4. Conclusions

In summary, we have successfully prepared new functionalized PMO nanocomposite films and powders with controlled structure and properties via EISA. This method allows for the in situ incorporation and chemical bonding of luminescent/charge transport functionalized materials inside the nanochannels of mesoporous organosilica using a simple spin-coating process. The resultant thin films show interesting photoluminescent and increased hardness properties over their nonordered counterparts to strongly suggest that the pore channels are occupied by the functionalized material of interest. We are currently investigating the PL and charge transport properties of thin films prepared by this process for potential application in organic light-emitting diodes (OLEDs), photovoltaics (OPVs), and thin-film transistors (OTFTs). Furthermore, we are exploring oxygen and water permeation properties of related nanocomposite thin films using MOCON for potential applications as barrier and abrasion-resistant films.

Acknowledgment. Financial support was provided by the Institute of Materials Research and Engineering (IMRE) and the Agency for Science, Technology and Research (A*STAR), Republic of Singapore. We thank Dr. Ping Yang from the Singapore Synchrotron Light Source (SSLS), Ms. Shue Yin Chow from IMRE, and Dr. Peter Sprenger from Bruker for their help with XRD, TEM, and ^{29}Si NMR experiments, respectively.

Supporting Information Available: FT-IR spectra of as-prepared and ethanol-washed pure PMO and PMO-(**3**) and ^{13}C CP MAS spectra of ethanol-washed pure PMO and PMO-(**3**).

CM702753B

(42) Hardness values are obtained from the following equation: $H = P/A_{max}$, where H = hardness, P = maximum indentation load, and A_{max} = maximum contact area.